Orthogonal and secondary concentration in planar micro-optic solar collectors

Jason H. Karp,* Eric. J. Tremblay, Justin M. Hallas, and Joseph E. Ford

Department of Electrical and Computer Engineering, University of California, San Diego, 9500 Gilman Drive, La Jolla, California 92093-0407, USA
**jkarp@ucsd.edu*

Abstract: Planar micro-optic concentrators are passive optical structures which combine a lens array with faceted microstructures to couple sunlight into a planar slab waveguide. Guided rays propagate within the slab to edge-mounted photovoltaic cells. This paper provides analysis and preliminary experiments describing modifications and additions to the geometry which increase concentration ratios along both the vertical and orthogonal waveguide axes. We present simulated results for a 900x concentrator with 85% optical efficiency, measured results for small-scale experimental systems and briefly discuss implementations using low-cost fabrication on continuous planar waveguides.

OCIS codes: (350.6050) Solar energy; (220.1770) Concentrators; (230.7400) Waveguides, slab; (080.1753) Etendue.

References and links

1. D. Feuermann and J. M. Gordon, "High-concentration photovoltaic designs based on miniature parabolic dishes," Sol. Energy **70**(5), 423–430 (2001).
2. A. Bett, C. Baur, F. Dimroth, G. Lange, M. Meusel, S. van Riesen, G. Siefer, V. Andreev, V. Rumyantsev, and N. Sadchikov, "FLATCON™-modules: technology and characterisation," WCPEC-3 634–637 (2003).
3. J. H. Karp, E. J. Tremblay, and J. E. Ford, "Planar micro-optic solar concentrator," Opt. Express **18**(2), 1122–1133 (2010).
4. J. C. Miñano, P. Benítez, J. Liu, J. Infante, J. Chaves, and L. Wang, "Applications of the SMS method to the design of compact optics," Proc. SPIE **7717**, 77170I, 77170I-8 (2010).
5. J. Chaves and M. Collares-Pereira, "Ultra flat ideal concentrators of high concentration," Sol. Energy **69**(4), 269–281 (2000).
6. C. Y. Chang, S. Y. Yang, and J. L. Sheh, "A roller embossing process for rapid fabrication of microlens arrays on glass substrates," Microsyst. Technol. **12**(8), 754–759 (2006).
7. S. H. Ahn and L. J. Guo, "High-Speed Roll-to-Roll Nanoimprint Lithography on Flexible Plastic Substrates," Adv. Mater. (Deerfield Beach Fla.) **20**(11), 2044–2049 (2008).
8. J. P. Morgan, "Light-guide solar panel and method of fabrication thereof," Morgan Solar, Inc. World Intellectual Property Organization, WO 2008/131561, 11 June 2008.
9. S. Ghosh and D. S. Schultz, "solar energy concentrator," Banyan Energy, Inc., Patent US 7,672,549B2, 2 March 2010.
10. B. L. Unger, G. R. Schmidt, and D. T. Moore, "Dimpled planar lightguide solar concentrators," in *OSA International Optical Design Conference,* ITuE5P (2010).
11. R. Sherif, R. King, N. Karam, and D. Lillington, "The path to 1 GW of concentrator photovoltaics using multijunction solar cells," IEEE PVSC **31**, 17–22 (2005).
12. W. T. Welford and R. Winston, *High Collection Nonimaging Optics* (1989).
13. H. Ries, "Thermodynamic limitations of the concentration of electromagnetic radiation," J. Opt. Soc. Am. **72**(3), 380 (1982).
14. A. Rabl, *Active Solar Collectors and their Applications* (Oxford University Press, 1985).
15. R. Winston and H. Hinterberger, "Principles of cylindrical concentrators for solar energy," Sol. Energy **17**(4), 255–258 (1975).
16. J. C. Miñano, J. C. Gonźlez, and P. Benítez, "A high-gain, compact, nonimaging concentrator: RXI," Appl. Opt. **34**(34), 7850–7856 (1995).
17. R. Winston, W. T. Welford, J. C. Miñano, and P. Benítez, *Nonimaging Optics* (Academic Press, 2005).
18. N. Fraidenraich, "Analytic solutions for the optical properties of V-trough concentrators," Appl. Opt. **31**(1), 131–139 (1992).

#141129 - $15.00 USD Received 14 Jan 2011; revised 21 Mar 2011; accepted 25 Mar 2011; published 17 May 2011

19. J. H. Karp, E. J. Tremblay, and J. E. Ford, "Radial coupling method for orthogonal concentration within planar micro-optic solar collectors," in *OSA Optics For Solar Energy*, STuD2 (2010).
20. M. Collares-Pereira, A. Rabl, and R. Winston, "Lens-mirror combinations with maximal concentration," Appl. Opt. **16**(10), 2677–2683 (1977).
21. A. T. Cannistra and T. J. Suleski, "Characterization of hybrid molding and lithography for SU-8 micro-optical components," J. Micro/Nanolith. MEMS MOEMS **9**(1), 013025 (2010).
22. J. H. Karp and J. E. Ford, "Planar micro-optic solar concentration using multiple imaging lenses into a common slab waveguide," Proc. SPIE **7407**, 7407–7411 (2009).
23. E. D. Palik, *Handbook of Optical Constants of Solids*, (Academic Press, 1998).
24. S. Van Gils, T. Dimogerontakis, G. Buytaert, E. Stijns, H. Terryn, P. Skeldon, G. E. Thompson, and M. R. Alexander, "Optical properties of magnetron-sputtered and rolled aluminum," J. Appl. Phys. **98**(8), 083505 (2005).
25. L. Fu, R. Leutz, and H. P. Annen, "Secondary optics for Fresnel lens solar concentrators," Proc. SPIE **7785**, 778509, 778509-6 (2010).

1. Introduction

Solar concentrators employ large optical components to focus sunlight onto small area photovoltaic cells. Concentrator photovoltaic (CPV) systems typically rely upon an array of lenses or mirrors which focus onto individual solar cells [1,2]. We previously introduced an ultrathin, planar concentrator which divides a single, large concentrating element into an array of millimeter-sized optics coupled to a common slab waveguide [3]. Each small aperture focuses onto localized fold mirrors embedded on the backside of a waveguide. These microstructures reflect light at angles that guide by total internal reflection (TIR), thereby coupling light from thousands of small apertures to a shared photovoltaic (PV) cell mounted at the edge(s). Other segmented-aperture optics have been proposed for concentration and lighting applications which use multiple discontinuous surfaces and can achieve significant reductions in total track length compared to the input aperture [4,5]. The planar micro-optic geometry described here differs in that all subapertures are repeatable and fabricated on a waveguide substrate of constant thickness, yielding an arrangement designed to be compatible with low-cost manufacturing techniques such as roll-to-roll processing [6,7].

The geometric concentration ratio associated with the basic planar micro-optic structure is defined by the waveguide length divided by two times the slab thickness, with no dependence on width. Microstructures on the waveguide surface couple light into the waveguide, but also strip guided rays upon subsequent interaction. The optical efficiency describes the percentage of light reaching the output and includes surface reflections, coating reflectivity, material absorption as well as decoupling losses associated with propagation. In high-concentration systems, downstream coupler interaction becomes the dominant loss mechanism. Though the geometric ratio between waveguide length and thickness can increase without bound, the output flux becomes saturated when propagation losses prevent light from additional lenses from reaching the output edge(s).

The intrinsic loss introduced by coupling microstructures can be managed through various waveguide and coupler geometries. Stepped or tapered waveguides have been proposed to reduce or eliminate interaction with lossy surface structures [8,9]. These systems can support efficient propagation, but large-area, three-dimensional components are not compatible with roll-to-roll manufacture and instead depend upon more costly molding processes. Another proposed approach to reduce propagation loss while maintaining a uniform thickness is to introduce bypass elements which divert guided light around coupling microstructures [10]. Bypass prisms can yield high efficiency at lower concentrations, but also enlarge the overall coupler area and increase the likelihood of downstream interaction. Because each bypass prism reflection adds to the angular spectrum of guided light, multiple prism reflections cause rays to break TIR and ultimately limit the concentration ratio.

Our planar micro-optic concentrator restricts coupling areas to a small percentage of the total waveguide surface by using a lens array to focus incident sunlight, as depicted in Fig. 1. The lens focal ratio (f-number or F/#) and solar acceptance angle determine the associated coupling area. The design requires accurate positioning between the lens array and coupling

#141129 - $15.00 USD Received 14 Jan 2011; revised 21 Mar 2011; accepted 25 Mar 2011; published 17 May 2011

microstructures. First, the coupler profile must be properly placed within the associated lens focus, and secondly, the overall lens array must be aligned to the patterned waveguide. In our experimental demonstrations, we address both alignment tolerances using a self-aligned fabrication approach wherein the shapes of the couplers are molded in photoresist covering the entire waveguide surface. Localized coupling regions are permanently formed using the lens array focal plane as a mask to selectively cross-link the resist when exposed to UV light. However, this process does not allow for active coupler placement within the focal region. In the systems modeled and characterized in this paper, we incorporate 120°-apex prisms with a spatial period smaller than the illuminated area to symmetrically tilt the focused light cone by ± 60° with respect to the top waveguide surface. Light can strike any portion of this periodic microstructure and couple into the waveguide without adjacent shadowing effects. We previously published a planar concentrator using F/2.45 lenses focusing onto 78μm diameter, 120° prisms fabricated onto a 1mm thick BK7 glass waveguide. Simulations suggested 81.9% optical efficiency at 300x concentration, with couplers occupying less than 0.1% of the 600mm diameter entrance aperture [3].

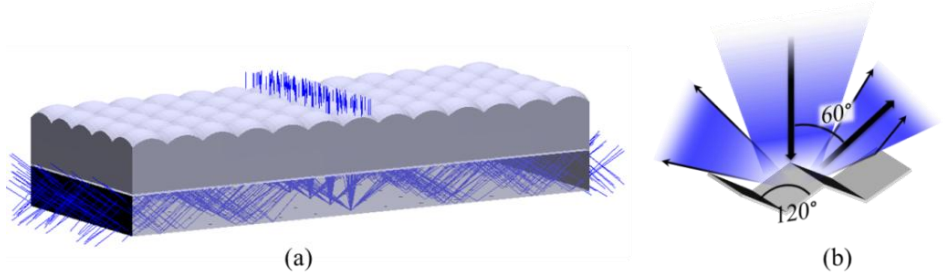

Fig. 1. The micro-optic concentrator pairs a lens array with a planar slab waveguide (a). Localized 120° prisms placed on the waveguide surface couple light into guided modes without shadowing effects (b).

Planar waveguides confine light within the slab thickness, yet require longer (or thinner) geometries to reach higher concentrations. Economics associated with CPV may encourage higher levels of concentration to reduce the quantities of costly semiconductor materials without sacrificing optical efficiency [11]. In this paper, we show how the waveguide geometry can be modified to incorporate concentration along the slab width as a means to increase concentration without incurring further propagation loss. Additionally, we show secondary optical elements situated between the waveguide edge and PV cell which provide extra concentration factors. In the following sections, we briefly review the limits of concentration and evaluate the angular spectrum of light exiting the waveguide. Sections 3 and 4 describe orthogonal waveguide concentration as well as present fabrication and experimental results for small-scale prototypes. Section 5 proposes a secondary optical element situated between two opposing concentrators and Section 6 describes possible combined configurations using both orthogonal waveguides and secondary optics. Conclusions are provided in Section 7.

2. Concentration limits

Étendue, a property of all optical systems, states that the product of the entrance pupil and source angle never increases [12]. Fundamentally, solar collectors must alter the angular spectrum of incident light in order to focus to smaller output apertures. The degree of concentration is limited by the second law of thermodynamics which requires heat to flow from a hot source towards a cooler body [13]. Equation (1) describes the two-dimensional and three-dimensional concentration limits in terms of acceptance angle, where θ_{in} is the source half angle [14]. At the thermodynamic limit, light fills the entire angular spectrum and exits the concentrator over ± 90°. Several optical geometries including compound parabolic

#141129 - $15.00 USD Received 14 Jan 2011; revised 21 Mar 2011; accepted 25 Mar 2011; published 17 May 2011

concentrators and nonimaging reflectors achieve this limit, however, practical concerns such as track length and complex fabrication can hinder real-world applications [15,16].

$$C_{2D} = \frac{1}{\sin\theta_{in}}, \qquad C_{3D} = \frac{1}{\sin^2\theta_{in}} \tag{1}$$

Planar micro-optic collectors offer thin profiles and simple fabrication, but fall short of the thermodynamic limit. As designed, imaging lenses are the only elements acting on incident solar angles and account for all observed concentration, however, imaging optics cannot reach the étendue limit [17]. Planar waveguides are used only to confine and transport coupled sunlight to the output(s). 120° prisms reflect converging light by 60°, after which rays diverge as they propagate within the slab. Depending upon an odd or even number of total reflections, light exits the waveguide at ± 30° with respect to the edge normal. Figure 2 traces coupled ray paths and graphs the output angular spectrum on a polar plot for F/3 lenses exiting a BK7 glass waveguide. If the concentrator were thermodynamically limited, rays would completely fill the polar plot, emitting over the entire hemisphere. However, the waveguide output occupies only a small fraction of the available angular spectrum, enabling additional forms of concentration that approach the theoretical limit.

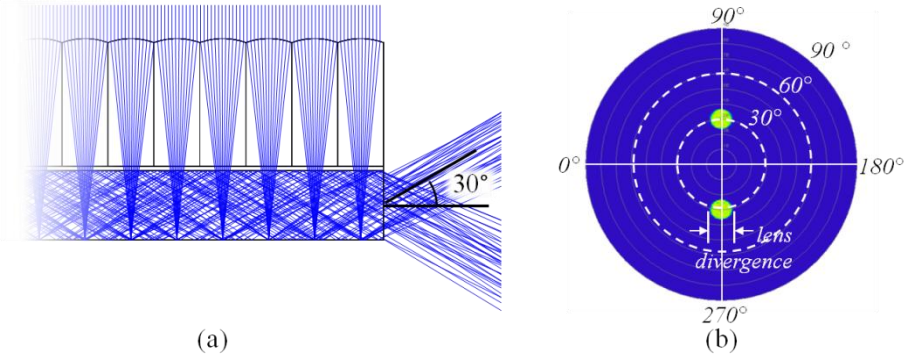

Fig. 2. The lens array and coupling prisms create two bundles exiting the waveguide (a). Within the polar plot, output angles (green circles) fill only a portion of the total angular spectrum (b).

3. Orthogonal waveguide concentration

3.1 Waveguide geometry

With rectangular waveguides, the geometric concentration ratio is only of function of length and thickness. Tilting the slab sidewalls with respect to the waveguide axis enables the slab to act as a v-trough concentrator and impart an additional concentrator factor along the slab width. Because the sidewalls restrict light in a manner perpendicular to confinement in thickness, we refer to this geometry as orthogonal waveguide concentration. Equation (2) revises the geometric concentration ratio to include concentration along the width where l and h describe the slab length and thickness and w_1 and w_2 represent the wide and narrow widths of the waveguide, respectively.

$$C_{geo} = \frac{l \cdot (w_1 + w_2)/2}{w_2 \cdot h} \tag{2}$$

One-dimensional v-troughs are one of the simplest concentrator configurations, but tend to reject rays after multiple reflections [18]. To reduce sidewall interaction, we oriented coupling prisms to preferentially reflect sunlight towards the output aperture [19]. Rotating the coupling direction as a function of position caused the geometry to appear as a lens focusing

#141129 - $15.00 USD Received 14 Jan 2011; revised 21 Mar 2011; accepted 25 Mar 2011; published 17 May 2011

into a v-trough, as shown in Fig. 3. The f-number of the equivalent lens and the sidewall angle influenced the orthogonal concentration factor and v-trough acceptance angle. Collares-Pereira et al. previously analyzed a cylindrical lens and v-trough combination which approached the thermodynamic limit in one dimension [20]. The authors developed their geometry using the well-known edge-ray principle proposed by Welford and Winston to ensure extreme rays reflected at ± 90° with respect to the output normal. All other angles fell within this output area, without rejection from multiple reflections.

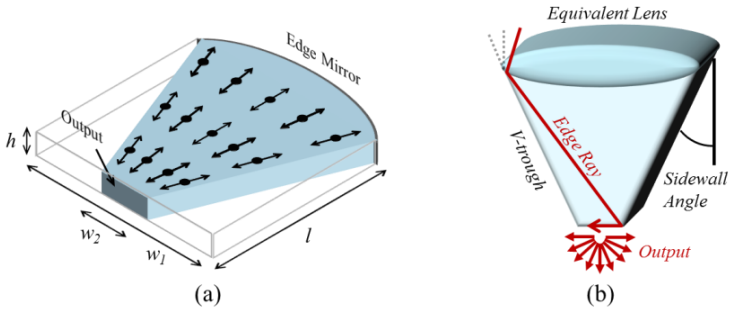

Fig. 3. Orthogonal waveguides provides additional concentration along the slab width (a). Radial coupler orientation appears as a lens focusing into a v-trough (b).

Figure 4 labels important dimensions of the v-trough geometry. The lens array collects solar angles θ and focuses into a waveguide of index n at a cone angle α. This divergence specifies the necessary acceptance angle of the v-trough. Equation (4) defines the v-trough aspect ratio solution calculated by Collares-Pereira et al, in terms of the thermodynamic limit C. The sidewall angle ψ and waveguide length l can be solved using Eqs. (5) and (6). Orthogonal waveguides with 120° microstructures require one key addition to capture light which initially couples away from the narrowed output. A parabolic reflector with focal length f integrated along the wide edge intercepts rays at near normal incidence and retroreflects them back towards the output. This mirror maintains the angular distribution of guided light, making the v-trough geometry suitable for both coupling directions.

$$\tan\alpha = \frac{1}{2\cdot F/\#} + \tan\theta \tag{3}$$

$$\frac{f}{w_i} = \frac{C+1}{2C^2}\left(3C^2 - 2C - 1\right)^{1/2} \quad \text{where} \quad C = \frac{w_i}{w_2} = \frac{1}{\sin\left(\alpha/n\right)} \tag{4}$$

$$\tan\psi = \frac{w_1}{2\cdot f} \tag{5}$$

$$l = f\left(1 - \frac{1}{C}\right) \tag{6}$$

#141129 - $15.00 USD Received 14 Jan 2011; revised 21 Mar 2011; accepted 25 Mar 2011; published 17 May 2011

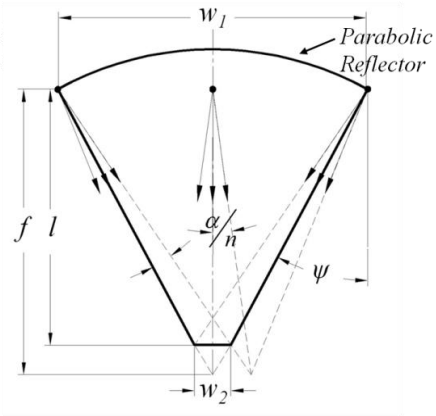

Fig. 4. Dimensions of the orthogonal waveguide layout.

3.2 Orthogonal concentration and f-number

We modeled orthogonal waveguide concentration for several lens array f-numbers using Zemax non-sequential ray tracing. All concentrators were based upon 200mm long, 1mm thick BK7 glass waveguides (n_d = 1.51), collecting ± 0.26° solar field angles. We assumed 95% coupler reflectivity while the waveguide and sidewalls were left uncoated. Though rays incident on the sidewalls appeared to exceed the critical angle, coupled light actually traveled along skew paths due to prism coupling and experienced TIR at the glass-air interface.

We observed different orthogonal concentration factors relating to the lens array f-number, as shown in Fig. 5. A system with F/1 optics focused light onto couplers covering 0.01% of the slab surface, yielding the highest initial efficiency prior to orthogonal concentration. Higher F/5 lenses required larger couplers covering 0.2% of the waveguide and reduced optical efficiency over 200mm of propagation. However, the focused cone associated with F/1 lenses spanned ± 18.4° in glass and limited the orthogonal concentration factor to 3.2x before rays broke TIR after multiple sidewall reflections. The narrower ± 3.9° cone angle associated with F/5 lenses pushed the orthogonal concentration factor to 14.5x before experiencing additional loss. At lower f-numbers, sidewall losses occurred abruptly whereas higher f-numbers more gradually lost efficiency and could be pushed beyond their calculated maximum. The combination of f-number, waveguide geometry and concentration ratio influence the desired layout of orthogonal planar concentrators.

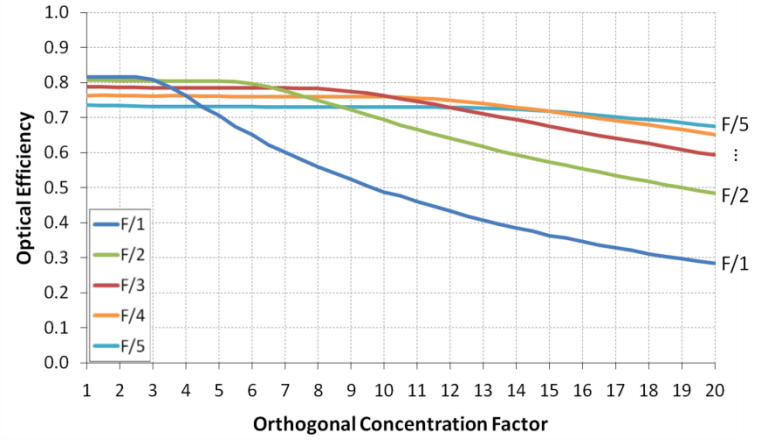

Fig. 5. Optical efficiency as a function of orthogonal concentration factor for various lens f-numbers. All systems incorporated 200mm of propagation in glass to the exit aperture.

#141129 - $15.00 USD Received 14 Jan 2011; revised 21 Mar 2011; accepted 25 Mar 2011; published 17 May 2011

3.3 Orthogonal vs. rectangular waveguides

We simulated micro-optic concentrators with F/3 lenses in both rectangular and orthogonal waveguide geometries. These particular lenses created ± 6.42° cone angles within the waveguide which enabled 8.93x orthogonal concentration. Collares-Pereira et al. noted off-axis aberrations caused some rays to deviate from their ideal path, leading to some loss prior to reaching the calculated limit. This effect lowered the realizable limit to 8x and can be seen in the previous figure.

Zemax simulations began with 200mm long, 1mm thick BK7 waveguides. In the orthogonal configuration, the concentration ratio was increased by reducing the output width. The rectangular waveguide reached higher concentrations by extending the slab length. From Eqs. (4) and (6), we calculated the wide and narrow widths of the waveguide at the orthogonal concentration limit to be 245.7mm and 30.7mm respectively. This increased the overall concentration ratio to 900x, prior to experiencing sidewall losses. The system maintained 85% optical efficiency up to this concentration, as shown in Fig. 6. By contrast, the rectangular system required an 1800mm long waveguide to reach 900x (concentration ratio equals waveguide length divided by two times the thickness, with light exiting opposing edges) which dropped the efficiency to 64.2% due increased propagation loss.

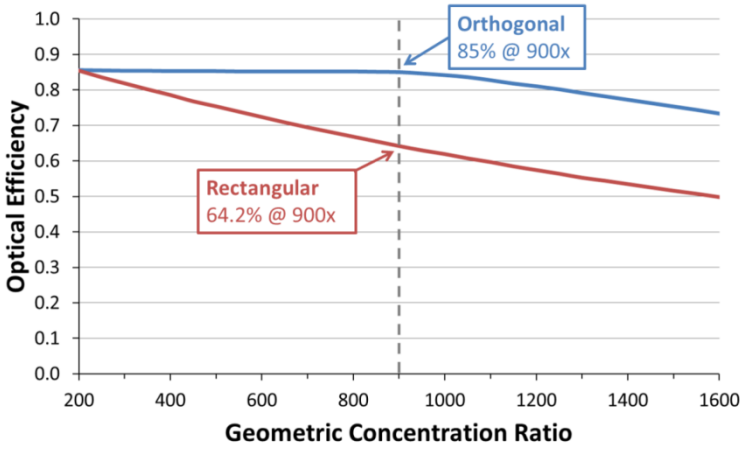

Fig. 6. Efficiency comparison between rectangular and orthogonal waveguide geometries. Both systems used an F/3 lens array and 1mm thick glass waveguides.

Orthogonal waveguides increase the concentration by acting on the angular spectrum of guided light. Figure 7 depicts the system aspect ratio at 8x orthogonal concentration, including a parabolic edge mirror represented as a Fresnel reflector. Note the number of lenses drawn in the figure have been reduced for visualization purposes. The polar plot shows an 8x increase in output angular spectrum, with rays occupying all angles one dimension. This example represents only one possible combination of lens f-number, acceptance angle and waveguide aperture with other combinations offering different orthogonal concentration ratios and efficiencies. The results cannot be compared directly to the ideal thermodynamic limit because micro-optic concentrators incorporate inherent loss mechanisms which must be included in the analysis.

#141129 - $15.00 USD Received 14 Jan 2011; revised 21 Mar 2011; accepted 25 Mar 2011; published 17 May 2011

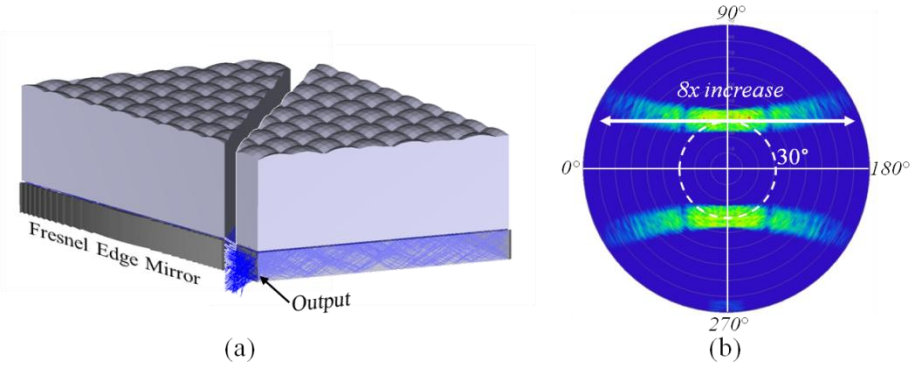

Fig. 7. Optical layout showing 8x orthogonal concentration using F/3 lenses (note: system scale has been reduced for visualization purposes) (a). Sidewalls confine light along the slab width, increasing the angular spectrum in one dimension (b).

4. Experimental prototypes

4.1 Self-aligned fabrication

We fabricated waveguide couplers as part of a small-scale prototype effort by adapting a SU-8 molding process developed by Cannistra et al. [21]. 50μm pitch, 120°-apex prisms were cast into a polydimethylsiloxane (PDMS) master mold and pressed into a 20μm thick SU-8 layer spun on the back waveguide surface. The mounted lens array focal plane selectively cross-linked the resist upon exposure to UV light [22]. We refer to this process as self-alignment because the lens array acts as the lithography mask, ensuring each coupler is matched in size and position to each lens element. The divergence of the UV light source determined the spot size formed by each lens. Setting the divergence to the angular extent of the sun created minimum coupling areas to maximize optical efficiency while expanding the divergence increased acceptance angles and relaxed solar alignment requirements. After exposure, we sputtered a reflective aluminum coating over the entire molded surface. With a combination of ultrasonics and heat in SU-8 developer, we successfully removed uncured resist, leaving reflective prisms precisely positioned at each lens focus. The process can potentially be adapted to use standard molding and roll-to-roll processing to yield inexpensive, large-aperture solar collectors.

4.2 Rectangular prototype

The following prototypes used commercially-available 1mm pitch, F/3.0 plano-convex lenses molded into a 3.3mm acrylic substrate. Lenses focused into a 75mm x 50mm x 1mm thick BK7 glass waveguide with 120° couplers fabricated on the back surface. The geometry yielded 37.5x geometric concentration at each of two outputs. Our first system maintained the rectangular waveguide geometry with 80μm diameter coupling prisms. Initial simulations predicted 76.2% optical efficiency at 37.5x, assuming 92% aluminum reflectivity and no antireflection coatings [23]. Due to the 50μm pitch of the prisms, 80μm coupling regions contained less than two prism periods. Light incident near the edge facet could refract through the coupler sidewall and enter the waveguide at an angle outside of the TIR condition. This loss mechanism in conjunction with measured 85% aluminum reflectivity reduced our simulated efficiency to 62.4%. Future systems should incorporate smaller prisms to reduce coupler edge loss as well as improve reflectivity through deposition process refinement [24].

The concentrator in Fig. 8 was tested using a Xe arc lamp collimated to approximate both the divergence and spectrum of the sun. Optical efficiency was measured using a 10mm x 10mm multijunction photovoltaic cell index-matched over a portion of one 50mm x 1mm output aperture. The cell was repositioned to several discrete locations along the slab edge to

#141129 - $15.00 USD Received 14 Jan 2011; revised 21 Mar 2011; accepted 25 Mar 2011; published 17 May 2011

account for the oversized output. By comparing the input illumination to the output, we experimentally measured 52.3% optical efficiency with ± 0.38° angular acceptance. Additional experimental losses were likely due to lens variations within the array, non-uniform reflector adhesion along the coupler perimeter and residual contaminants on the waveguide surface which adversely affected TIR.

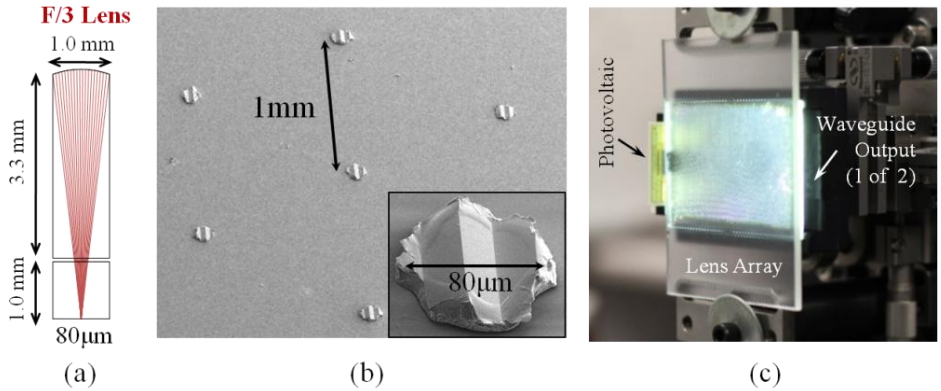

Fig. 8. Optical layout of the prototype concentrator (a). SEM image of the waveguide surface showing coupler spacing and diameter (inset) (b). Image of the system under test (c).

4.3 Orthogonal waveguide prototype

To demonstrate orthogonal waveguide concentration, we diced the rectangular slab to create 11.3° trough angles and a single, 20mm x 1mm output aperture. This conservative geometry sat well below the orthogonal concentration limit and was chosen to relax coupling angles and component integration. We approximated radial coupler orientation using three assembled sections of a linear 120° prism array, as shown in Fig. 9. Instead of a parabolic mirror integrated into the slab, the narrow trough angle enabled a planar mirror to be index-matched along the wide edge. The last modification involved polishing the waveguide sidewalls which were diffuse after dicing. As an alternative to difficult edge polishing, we bonded a thin layer of PDMS along the edge. This simple approach refaceted the sidewalls by index-matching to a planar edge surface, effectively removing surface irregularities. We modeled the orthogonal geometry using identical lenses, couplers, prisms and mirror reflectivity found in the rectangular setup. Simulations yielded 131x geometric concentration with 59.4% optical efficiency. The performance was slightly below that of rectangular systems due to an additional reflection off the 85% reflectivity edge mirror.

To measured optical efficiency, we mounted a 30mm x 3mm photodiode along the output an collected all the light exiting the system without repositioning. We experimentally measured 22.4% optical efficiency when illuminated with the Xe solar simulator. This measurement was significantly lower than expected and was attributed to several loss mechanisms unique to the orthogonal waveguide setup. Though refaceting the sidewalls with PDMS left specular edges, point defects and chips in the glass allowed light to escape the waveguide. Refaceting also left residual material along the waveguide edges leading to additional loss at the sidewall corners. Similar losses occurred at the back edge reflector with small amounts of index gel overflowing onto the top and bottom waveguide surfaces after assembly. For orthogonal concentration to reach its simulated potential, these surface quality and assembly issues must be addressed. In Section 6.2, we propose equivalent microstructures placed on the bottom waveguide surface which impart orthogonal concentration without polishing or assembly losses.

#141129 - $15.00 USD Received 14 Jan 2011; revised 21 Mar 2011; accepted 25 Mar 2011; published 17 May 2011

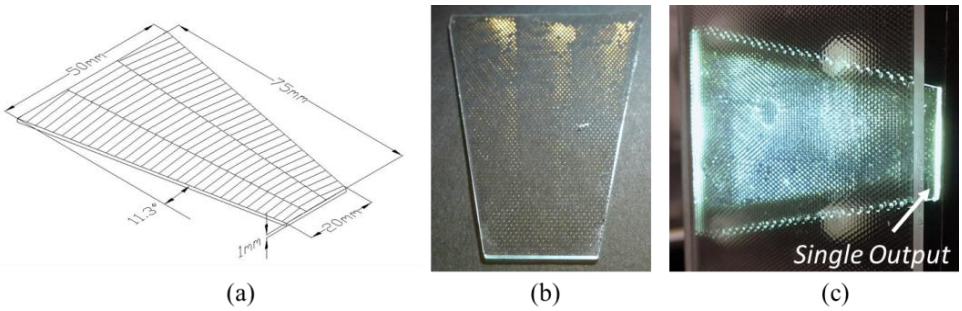

Fig. 9. Geometry of the experimental orthogonal concentrator (a). Image of the fabricated waveguide (b) and the concentrator under test (c).

5. Secondary optical element

5.1 Design

CPV systems often incorporate secondary optical elements (SOE) such as kaleidoscopes or compound parabolic concentrators to provide additional light confinement [25]. Here, we describe a SOE situated between two opposing waveguides which captures and concentrates the unique angular distribution at the waveguide outputs. Light approaching the slab edge experiences either an odd or even number of total TIR reflections, producing two distinct ray bundles biased at ± 30° with respect to the waveguide axis. The SOE drawn in Fig. 10 uses a planar bottom surface to reflect odd-numbered rays, depicted in green, back upwards so all exiting rays see an even number of total reflections. Upward-emitting rays, traced in blue, avoid this bottom surface. The two parallel bundles strike a decentered parabolic mirror and focus onto a PV cell situated beneath the SOE. The mirror axis is centered atop the opposing waveguide and tilted by 30° to minimize path length. Since light approaches the SOE from both sides, a second reflector intercepts light from the opposing waveguide and focuses onto the same output.

The SOE also supports a second nonimaging ray path for light undergoing an odd number of TIR reflections. Downward propagating rays can reach the PV cell directly, without reflecting off the planar surface or parabolic mirror. This path is analogous to light traveling down the center of a kaleidoscope, avoiding interaction with the sidewalls. Nonimaging rays account for the extreme, downward light path and mark one of the output boundaries. Upward-propagating marginal rays correspondingly represent edge rays, also highlighted in red, and define the other output boundary. The SOE can be considered a variation of the compound parabolic concentrator, however, opposing entrance apertures prohibit light from exiting at the thermodynamic limit.

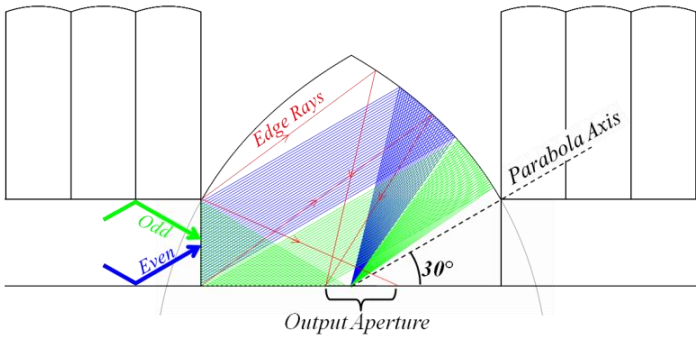

Fig. 10. Layout of the SOE positioned between two opposing waveguides.

#141129 - $15.00 USD Received 14 Jan 2011; revised 21 Mar 2011; accepted 25 Mar 2011; published 17 May 2011

5.2 Simulation

We simulated a waveguide SOE collecting light from concentrators using F/3 lens arrays. Aspheric surface coefficients were added to the parabolic reflector to help balance off-axis aberrations. After optimization, the SOE focused sunlight to an exit aperture 3.3x smaller than the combined waveguide areas with >99% of rays reaching the output. The optical efficiency of the system depended largely upon mirror reflectivity, with metallic reflectors being >90% and dielectric stacks approaching 99%. In terms of angular spectrum, rays approaching the PV cell spanned ± 12° to ± 65°, shown in Fig. 11. Similar layouts can be designed using other lens f-numbers, however, the resulting concentration factor will vary proportionally.

Placing the SOE between two waveguide concentrators has the added benefit of repositioning the PV cell beneath the waveguide. With the cell underneath, the carrier, heatsink and electrical interconnects can be incorporated without obscuring the collection aperture. This particular SOE design can be molded as a separate glass element, likely affixed to the PV cell prior to mating to the waveguides.

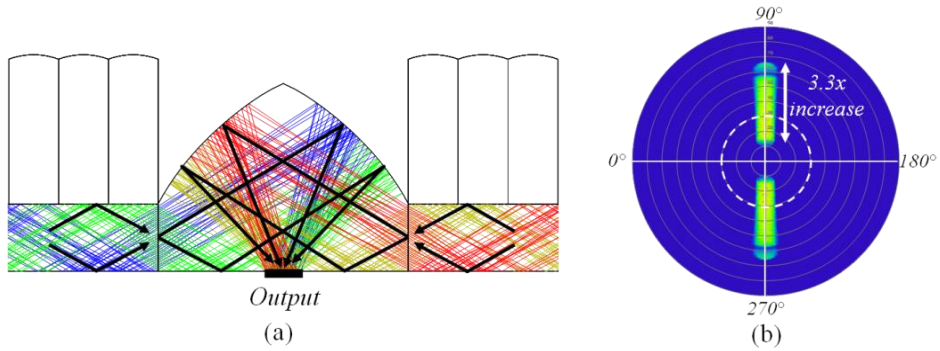

Fig. 11. Raytrace highlighting the odd and even reflection ray paths within the SOE (a) and the associated angular spectrum when capturing the output from F/3 focusing lenses (b).

6. System implementations

6.1 'Bowtie' combination

Orthogonal waveguides and secondary optics both increase the concentration ratio by acting on the angular spectrum, but in perpendicular directions. Both approaches can therefore be combined within the same system to reach even higher concentration levels. The joint configuration positions two orthogonal waveguides to form a 'bowtie', mating to a SOE at the center. Simulating two 900x orthogonal waveguide concentrators with a 3.3x SOE yielded 2970x geometric concentration with >80% optical efficiency. Figure 12 depicts the combined system along with the two-dimensional increase in angular spectrum. Note the SOE must include reflective sidewalls to confine light diverging from the output.

Very high concentration ratios can lead to practical concerns such as heat and angular acceptance at the PV cell. Instead of maximizing concentration, the combined system can be designed to operate at lower flux levels in exchange for increased acceptance angle or reduced output angular spectrum. Optimization between lens f-number, coupler area, waveguide geometry and secondary optics yield significant flexibility within these proposed designs.

#141129 - $15.00 USD Received 14 Jan 2011; revised 21 Mar 2011; accepted 25 Mar 2011; published 17 May 2011

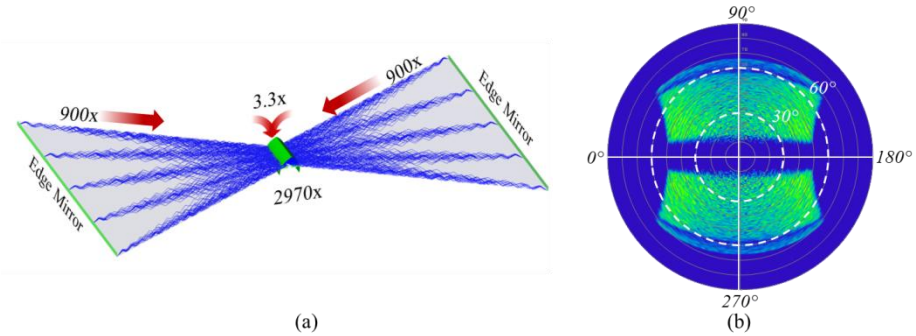

Fig. 12. Orthogonal waveguides can be combined with secondary optics to reach very high concentration levels (a). The associated angular spectrum increases in two dimensions (b).

6.2 Planar equivalent

As described, orthogonal waveguides and SOEs are no longer compatible with continuous roll-to-roll manufacturing. The layout contains several individual components which must be polished and assembled with high precision. Interestingly, orthogonal waveguides can be imposed onto rectangular substrates by replacing angled sidewalls and back reflectors with equivalent micro-optics embossed on the slab surface. Figure 13 describes a planar micro-optic concentrator using both orthogonal concentration and secondary optics placed on a continuous waveguide. Prismatic arrays create virtual sidewalls which reflect light into the v-trough without perpendicular edges. Edge-mounted reflectors can be replaced with surface-mounted Fresnel mirrors which direct light coupled away from one output to the adjacent exit aperture. Lastly, revised SOEs index-matched to the bottom surface extract guided light at specific locations and couple to the PV cell. These microstructures (except for SOEs) can be fabricated in tandem with 120° prism couplers, allowing the waveguide and lens array to remain continuous. Replacing edge-mounted optics with planar equivalents also avoids dicing and polishing steps which reduced efficiency in our experimental prototypes. However, planar optics impose additional constraints involving field angles and shadowing and should be designed in conjunction with the lens f-number and v-trough angle.

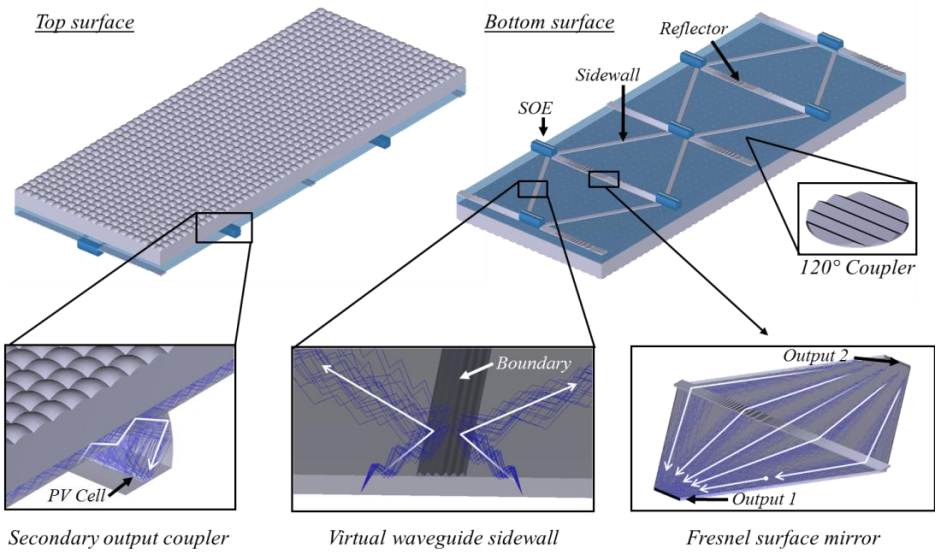

Fig. 13. Equivalent micro-optics increase concentration without sectioning the lens array or waveguide and enable continuous manufacturing approaches.

#141129 - $15.00 USD Received 14 Jan 2011; revised 21 Mar 2011; accepted 25 Mar 2011; published 17 May 2011

7. Conclusion

Micro-optic concentration confines light collected from thousands of small-aperture lenses within a common planar waveguide. The research included in this paper explored approaches to increase the geometric concentration ratio without incurring additional losses associated with waveguide propagation. The nominally rectangular waveguide was redesigned to appear as a lens focusing into a v-trough collector in order to confine light along the slab width in addition to its thickness. By properly selecting the aspect ratio and trough angle, the geometry approached the thermodynamic limit in one dimension, with an equal increase in output angular spectrum. A simulated system using F/3 lenses was capable of 8x additional concentration along the waveguide width resulting in a 900x concentrator with 85% optical efficiency. Secondary optical elements supplemented orthogonal waveguides by interfacing between two opposing outputs and repositioning the PV cell beneath the slabs. These additional concentration methods were unique to this planar geometry because the initial design utilized only a small percentage of the available angular spectrum.

We also presented experimental efficiency measurements for rectangular and orthogonal waveguide prototypes fabricated by self-aligned lithography. The rectangular geometry reached 52.3% optical efficiency which was comparable to simulated results. Sectioning the waveguide into a v-trough required sidewall polishing and component assembly which resulted in and additional losses. However, these experimental concentrators demonstrated low-cost fabrication steps which can be improved to approach simulated performance with further industrial development. Future systems may use equivalent micro-optics molded on the backside of continuous waveguides to impart orthogonal concentration without dicing, polishing or assembly. Orthogonal confinement and secondary optics provide additional degrees of freedom when designing high-concentration, high-efficiency planar collectors compatible with volume manufacture.

#141129 - $15.00 USD Received 14 Jan 2011; revised 21 Mar 2011; accepted 25 Mar 2011; published 17 May 2011